Small-scale intermittency in anisotropic turbulence

Wouter J. T. Bos, Lukas Liechtenstein, and Kai Schneider
MSNMGP, CNRS & CMI, Université de Provence, Marseille, France
(Received 27 April 2007; revised manuscript received 31 August 2007; published 10 October 2007)

Isotropic, rotating, and stratified turbulent flows are analyzed using a scale- and direction-dependent flatness. The anisotropy of the spatial fluctuations of the energy distribution can hereby be quantified for different length scales. This measure allows one to distinguish between longitudinal and transversal intermittency as well as between horizontal and vertical intermittency. The difference between longitudinal and transversal intermittency is argued to be related to the incompressiblity constraint. A large difference between horizontal and vertical intermittency for stratified turbulence can be explained by an energy depletion of the horizontal plane in Fourier space.

DOI: 10.1103/PhysRevE.76.046310 PACS number(s): 47.27.Gs, 47.32.Ef

I. INTRODUCTION

Turbulence in geophysical flows—e.g., in the atmosphere or in the ocean—is generally anisotropic due to the presence of shear, rotation, and stratification. In these flows the modeling and understanding of anomalous transport of pollutants needs knowledge of small-scale intermittency. In the present work, by intermittency we mean small-scale activity, localized in space. Intermittency has been studied since its introduction by Taylor [1]. Townsend [2] was the first to introduce a measure for small-scale intermittency, the flatness. Subsequently, to study the variation of intermittency with scale, Sandborn introduced a quantitative measure, the scale-dependent flatness [3], and showed that for intermittent flows the flatness strongly increases with wave number.

Batchelor and Townsend [4] explained intermittency by the presence of coherent structures. As in turbulence the coherent structures reflect the anisotropy (e.g., vortex tubes aligned with the rotation axis in rotating turbulence and horizontal vortex sheets in stably stratified turbulence as shown in Fig. 1), the intermittency can be expected to be anisotropic. This issue, the anisotropy of small-scale intermittency, will be addressed in the present work.

To study anisotropic turbulence specific tools are needed. Progress has been made, notably by using directional energy spectra ([5–7] and references therein). Directional spectra, while capturing the multiscale character, cannot quantify the spatially intermittent nature of the flows. Indeed, the intermittency related to spatially localized events is hidden in the phase of the Fourier modes. It was argued by Brun and Pumir [8] that when the largest turbulent scales are well resolved—i.e., when the domain-size is much larger than the correlation length—intermittency is only observable in the dissipation range. This dissipation range intermittency was predicted by Kraichnan [9]: in the highest wave number range, where viscous dissipation smoothens the fluctuations, the distribution of energy shows a very fast falloff. In this range, small variations of the cutoff scale, corresponding to the different flow structures or regions, lead to tremendous relative fluctuations of the turbulent intensity.

If in addition to dissipation range intermittency inertial range intermittency is of interest, Fourier modes are not the adequate basis functions. Wavelet coefficients are then more appropriate, because they conserve information on the localization in physical space. Another method is the use of structure functions, in particular within the context of the SO(3) decomposition [10]. However, structure functions can yield erroneous scalings if the considered velocity field is too smooth or too irregular [11,12]. Indeed, structure functions are closely related to wavelets [12], which do not have this disadvantage, but conserve the other advantages of structure functions: they can simultaneously address the multiscale distribution of a quantity, its anisotropy, and yield information on its spatial distribution. In the present work we therefore use wavelets and in particular a statistical tool is introduced, the scale-dependent directional flatness, inspired by the work of Meneveau [13] and Farge *et al.* [14], who used

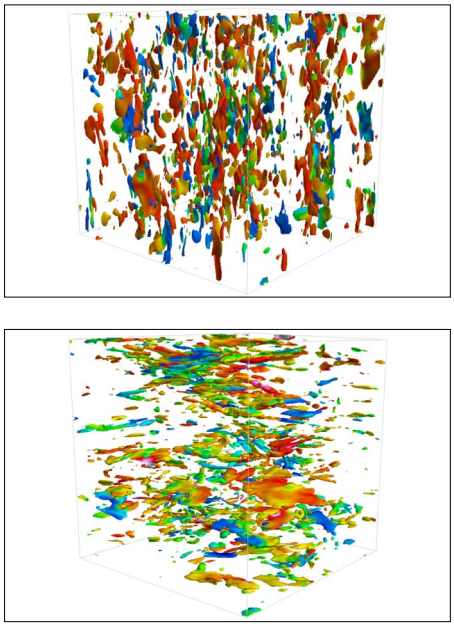

FIG. 1. (Color online) Isoenstrophy surfaces from direct numerical simulation for rotating (top) and stratified (bottom) turbulence with an isovalue equal to the mean enstrophy. In the rotating case we observe elongated vertical structures, in the stratified case flattened horizontal structures. The vertical velocity is shown in the visualization by a color scale (online only) ranging from blue (negative velocity) to red (positive velocity).

TABLE I. Sets of parameters of the three DNS runs. $\mathcal{T}_0$ indicates after how many turnover times the data are evaluated.

	e	$\mathcal{L}$	R_λ	Ro or Fr	Time ($\mathcal{T}_0$)
Isotropic	0.014	0.37	34		6
Rotating	0.034	0.37	60	Ro=0.025	3
Stratified	0.056	0.44	121	Fr=0.028	11.5

three-dimensional orthogonal wavelets and two-dimensional angle-dependent continuous wavelets, respectively. The scale-dependent directional flatness can be seen as an anisotropic extension of the spectral flatness [8,15,16], applied to scale space rather than to Fourier space.

In the next section we will describe the direct numerical simulations that yield the velocity fields analyzed in this work. Subsequently, in Sec. III we will discuss the link between wavelet space and Fourier space. In Sec. IV we analyze the velocity fields using two measures: the directional energy and the scale-dependent directional flatness. It is shown that a large part of the observed anisotropy of the energy distribution is due to the incompressibility constraint. Finally, it is argued that the anisotropic small-scale intermittency can be explained by the competition of various mechanisms: dissipation range fluctuations, incompressibility, and body forces.

II. DIRECT NUMERICAL SIMULATIONS

We consider velocity fields obtained by direct numerical simulation (DNS) of Navier-Stokes turbulence, using a classical pseudospectral method. Anisotropy is created by rotation and stratification, both oriented along the vertical axis. The velocity fields considered here correspond to decaying isotropic, rotating, and stably stratified incompressible turbulence within the Boussinesq approximation using 512^3 grid points. No external forcing is applied to the velocity fields, so that the Reynolds number is moderate and the inertial range is not well pronounced. However, forcing is known to affect the anisotropy induced by the body forces. To avoid artifacts caused by the forcing, the freely decaying case is considered. The parameters are summarized in Table I. Specific attention has been paid to the large scale anisotropy of the flow: the Froude and Rossby numbers are comparable. These quantities are defined as $\mathrm{Fr}=\mathcal{U}/\mathcal{L}N$ and $\mathrm{Ro}=\mathcal{U}/\mathcal{L}f$, with N and f being the Brunt-Väisälä frequency and rotation number, respectively. Here the integral turbulent velocity $\mathcal{U}$ and the integral length scale $\mathcal{L}$ are defined as

$$\mathcal{U}=\sqrt{2e/3}, \quad \mathcal{L}=\frac{\pi}{2\mathcal{U}^2}\sqrt{\int \frac{E(k)}{k}dk}, \tag{1}$$

with $e=\int E(k)dk$ and $E(k)$ the spherically averaged energy spectrum. The Reynolds numbers, based on the Taylor-microscale [$R_\lambda=\sqrt{20e^2/(3\nu\epsilon)}$, with ν the kinematic viscosity and ϵ the dissipation of kinetic energy], are of the same order of magnitude. For details about the method and the setup of the simulations, we refer to [17]. In addition to these three cases a vector-valued test field was generated consisting of divergence-free Gaussian white noise, with $E(k)\sim k^2$.

III. WAVELET SPACE AND ITS RELATION TO FOURIER SPACE

The velocity field at a given time instant is projected onto an orthogonal wavelet basis (see, e.g., [18] for details). We use Coiflet-12 wavelets, which have four vanishing moments and a filter length of 12. The projection of one component $u(\boldsymbol{x})$ of a vector field $\boldsymbol{u}=(u,v,w)$ onto orthogonal wavelets $\psi(\boldsymbol{x})$ can be represented by

$$u(\boldsymbol{x})=\sum_\lambda \tilde{u}_\lambda \psi_\lambda(\boldsymbol{x}), \tag{2}$$

with the subscript $\lambda=(j,\boldsymbol{i},d)$, where j represents the scale, $\boldsymbol{i}$ the position, and d the direction. The coefficients are stocked in a 512^3 wavelet space. The orthonormal character of the wavelets implies that for a data field of $N^3=2^{3J}$ values, j takes the values $j=\{0,1,\ldots,J-1\}$. In the wavelet representation seven spatial directions can be defined in three space dimensions (in D dimensions, 2^D-1 directions exist). For every particular combination of scale j and direction d, $\boldsymbol{i}$ can take 2^{3j} different values, which give an information on the localization in physical space. The parameters $(j,\boldsymbol{i},d)$ are then equivalent to coordinates in wavelet space. This wavelet space, in the Mallat representation [19], is shown in Fig. 2 as compared to Fourier space for both two and three dimensions. Hereby a direct link is shown between the two approaches. The dashed part of wavelet space, corresponding to one of the seven spatial directions (in three dimensions), is associated with the dashed part of Fourier space in the figures: it constitutes an orthogonal partition of Fourier space. Each individual box in wavelet space corresponds to a direction d and a scale j. Each scale can be linked to a wave number k_j by

$$k_j=k_0 2^j, \tag{3}$$

with

$$k_0=\frac{\int_0^\infty k|\hat{\psi}(k)|dk}{\int_0^\infty |\hat{\psi}(k)|dk},$$

where k_0 is the centroid wave number, a constant for each type of wavelet ($k_0\approx 0.77$ for Coiflet-12). It is hereby possible to reconstruct an energy spectrum by calculating the spectral energy density corresponding to a mean wave number k_j. The relation is

$$\tilde{E}(k_j)=\alpha_j\langle e_\lambda\rangle_{(j)}, \tag{4}$$

with

$$e_\lambda=(\tilde{u}_\lambda^2+\tilde{v}_\lambda^2+\tilde{w}_\lambda^2)/2,$$

in which the averaging has been performed over the position $\boldsymbol{i}$ and the direction d and with $\alpha_j=4\pi 2^{2j}/(7k_0)$ a scale-

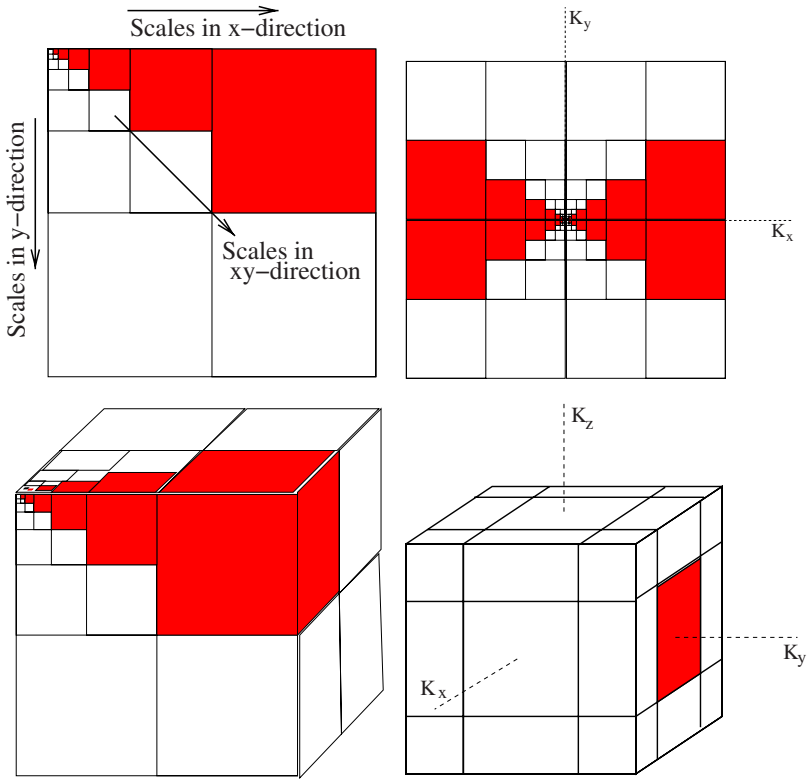

FIG. 2. (Color online) Left: wavelet space in two and three dimensions. Right: wavelet space projected onto Fourier space. Each box corresponds to a certain scale j and direction d, and each box contains 2^{2j} values of $\boldsymbol{i}$ in two dimensions and 2^{3j} in three dimensions, giving information on localization in physical space. Hereby we can relate a scale j to a wave number k_j: $k_j = k_0 2^j$, where k_0 is the centroid wave number of the wavelet.

dependent factor relating the discrete wavelet representation to spherical shells in Fourier space. This approach was initially proposed by Meneveau [13], and for further details we refer to his pioneering work. The disadvantage of these wavelet based energy spectra is the loss of spectral resolution: the spectrum contains one point for each scale j—that is, for each octave. This loss of information is, however, compensated for by information on the spatial variance of the energy spectrum, because for every scale j (corresponding to seven boxes), we have $2^{3j} \times 7$ values. The spatial variation can be expressed as the standard deviation of the spectral distribution. This standard deviation is defined by

$$\sigma_{\tilde{E}}(k_j) = \alpha_j [\langle e_\lambda^2 \rangle_{(j)} - \langle e_\lambda \rangle_{(j)}^2]^{1/2}. \tag{5}$$

In Fig. 3 both the spherically averaged Fourier energy spectrum $E(k)$ and the wavelet spectrum $\tilde{E}(k_j)$ are shown for isotropic turbulence. The wavelet spectrum agrees well with the Fourier spectrum. The spatial variation of the spectral distribution is shown in Fig. 3 by adding the points that indicate the spectrum plus one standard deviation $[\tilde{E}(k_j) + \sigma_{\tilde{E}}(k_j)]$. This variation is closely related to the flatness as will be explained in the following.

IV. ANALYSIS OF THE ANISOTROPY OF THE VELOCITY FIELDS

A. Directional energy

Because of incompressibility, the energy distribution in Fourier space of an isotropic vector-field can be expressed as

$$\Phi_{ij}(\boldsymbol{k}) = \left(\delta_{ij} - \frac{k_i k_j}{k^2} \right) \frac{E(k)}{4\pi k^2}, \tag{6}$$

which means that for a certain component [for example, $\Phi_{11}(\boldsymbol{k})$] one finds

$$\Phi_{11}(\boldsymbol{k}) = \left(1 - \frac{k_1 k_1}{k^2} \right) \frac{E(k)}{4\pi k^2} = \sin^2 \phi \, \frac{E(k)}{4\pi k^2}, \tag{7}$$

with ϕ the angle between the wave vector and the k_x axis. This results in an 8-shaped distribution in two dimensions, shown in Fig. 4. In three dimensions this 8-shaped distribution is rotated around the k_x axis for $\Phi_{11}(\boldsymbol{k})$. This leads to an anisotropy in the directional energy of the vector field com-

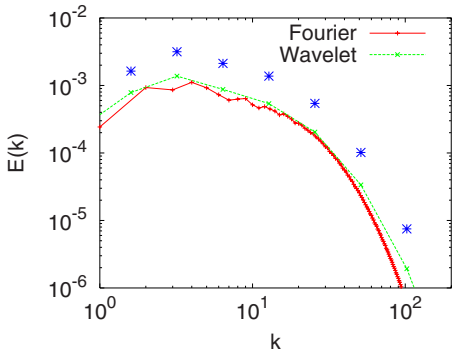

FIG. 3. (Color online) The (Fourier) energy spectrum for isotropic turbulence. Also shown is the dual spectrum constructed from wavelet coefficients. The stars indicate the standard deviation of the spatial distribution of the spectral energy density.

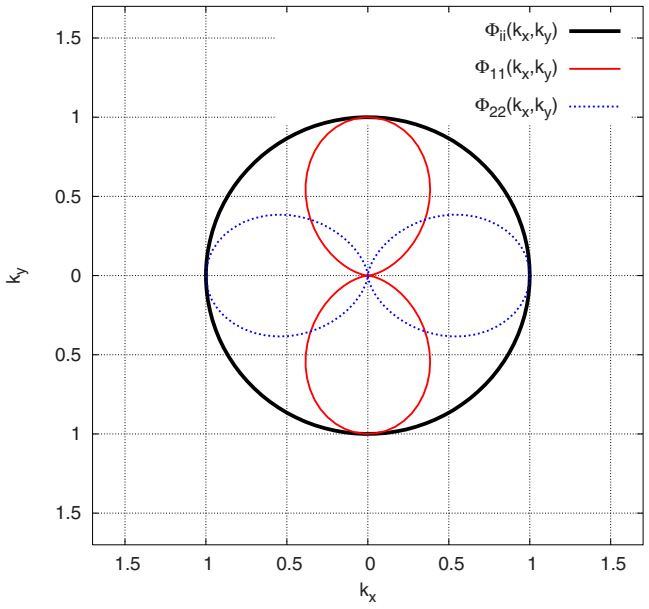

FIG. 4. (Color online) The variance of individual components of a divergence-free isotropic vector field is not isotropically distributed. Isovalues of two components $\Phi_{11}(\boldsymbol{k})$ and $\Phi_{22}(\boldsymbol{k})$ are plotted as well as their isotropic sum.

ponents, even for isotropic fields. Rotation or stratification can amplify or reduce this effect.

The general picture that emerges from studies using directional spectra [6,20] is that in stratified turbulence the kinetic energy is concentrated in a cone around the vertical axis of Fourier space. For rotating turbulence, the inverse tendency, an accumulation of energy close to the horizontal plane in Fourier space, is observed. In physical space this energy distribution corresponds to sheetlike structures in stratified turbulence and vertical vortex tubes in rotating turbulence, as illustrated in Fig. 1. The distribution of energy in wavelet space—i.e., the wavelet coefficients in the different boxes—allows a direct quantification of anisotropy. The directional energy $e_{(d)}$ is obtained by summing the energy over all boxes in wavelet space in a particular direction (illustrated in Fig. 2, on the left, for a horizontal direction). It can be stressed here that the vertical direction in wavelet space contains a particular discrete dyadic cone in Fourier space around the k_z axis, similar to the cones in [6,20]. We can therefore anticipate that the energy in this direction will be reduced in the rotating case and enhanced in the stratified case.

In Fig. 5 the directional energy is shown for the three different velocity components u, v, and w as a percentage with respect to the total energy of $\boldsymbol{u}$. In the present work we focus on the three principal directions x, y, and z. The four diagonal directions, which contain the remaining part of the energy, are not shown. For the divergence-free Gaussian noise, if one considers one velocity component, the directional distribution is not isotropic. Longitudinal energy (e.g., u in the x direction) is smaller than the transversal components (e.g., u in the y direction). The reason for this is the incompressibility constraint, as illustrated in Fig. 4: the Riesz projector reduces the energy in the longitudinal direction in favor of the transversal ones. The directional energy of isotropic turbulence behaves very similar to the Gaussian field: the longitudinal energy is smaller than the transversal energy. For rotating turbulence we see a similar picture, even though the directional energy is reduced in the z direction. Indeed, the formation of columnar structures reduces the spatial variation in this direction. The reduction of the energy in the z direction is, however, moderate and two-dimensionalization is not achieved. The picture is dramatically different for stratified turbulence in which all components are reduced in favor of the u and v energy in the z direction. This energy distribution clearly corresponds to a vertically sheared horizontal flow. The flow is close to the two-component limit.

B. Directional flatness

The standard deviation of the spatial distribution of the scale-dependent energy involves the square root of fourth-order moments of the wavelet coefficients. It can be directly related to the flatness. For a component u of the velocity field we introduce the directional scale-dependent flatness

$$F^u_{(j,d)} = \frac{\langle \tilde{u}^4_\lambda \rangle_{(j,d)}}{\langle \tilde{u}^2_\lambda \rangle^2_{(j,d)}}, \tag{8}$$

in which averaging is performed only over the position $\boldsymbol{i}$. This can be related to the standard deviation of the spectral distribution of u by

$$F^u_{(j,d)} = \left(\frac{\sigma_{\tilde{E}_u}(k_j,d)}{\tilde{E}_u(k_j,d)} \right)^2 + 1, \tag{9}$$

in which the spectrum $\tilde{E}_u(k_j,d)$ and its standard deviation $\sigma_{\tilde{E}_u}(k_j,d)$ are defined as in (4) and (5) by using only one component of the velocity in one direction d of wavelet space. The scale-dependent directional flatness is thus a mea-

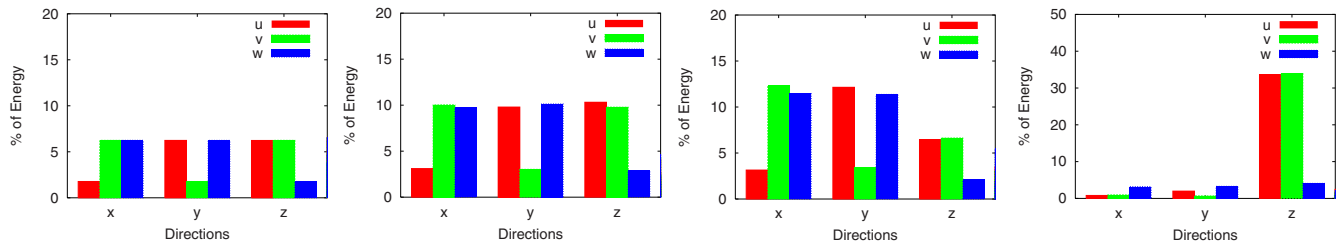

FIG. 5. (Color online) Directional energy of the three velocity components u, v, and w for (from left to right) divergence-free Gaussian white noise and isotropic, rotating, and stratified turbulence.

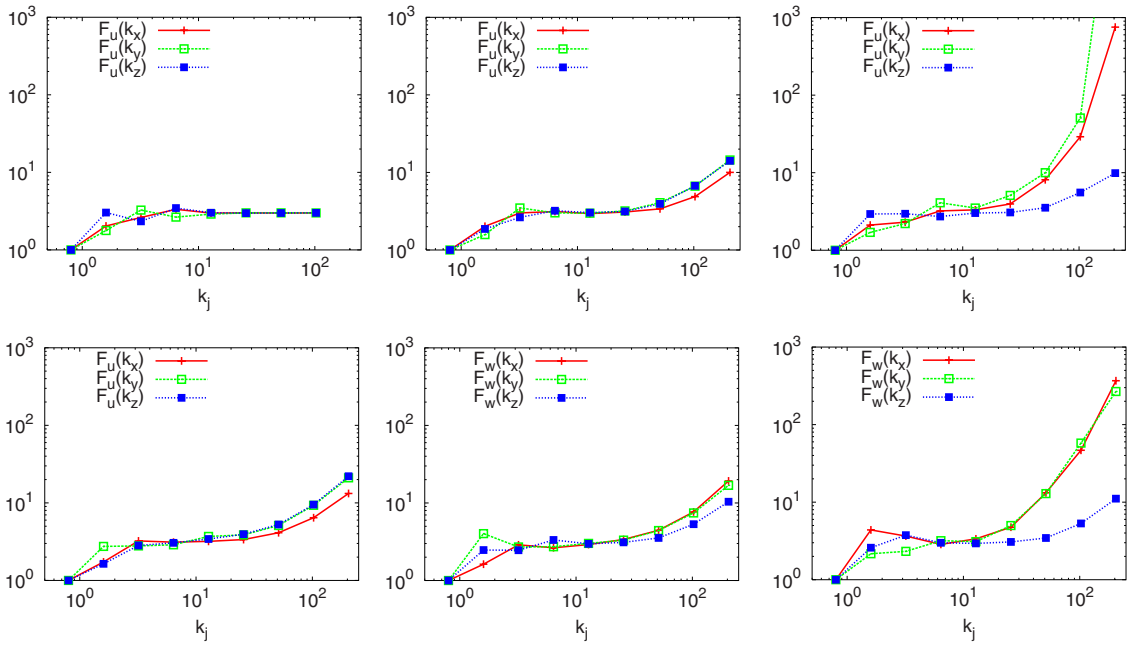

FIG. 6. (Color online) Directional scale-dependent flatness for Gaussian white noise (left top) and isotropic turbulence, u component (left bottom); rotating turbulence, u and w components (middle); and stratified turbulence, u and w components (right).

sure for the relative spatial fluctuation of the directional spectral energy density. It should therefore be an adequate measure for intermittency in the sense of Kraichnan [9]: extreme relative intensity fluctuations at small scales should translate into large deviations of $F^{u}_{(j,d)}$ from its Gaussian value of 3. Furthermore, the physical space locality of the wavelets should allow us to investigate inertial range intermittency if the Reynolds number is sufficiently high.

In Fig. 6 the directional flatness is plotted versus wave number for the different flow fields. For the divergence-free Gaussian white noise, the flatness is as expected equal to 3. For all the other flows the intermediate scales are close to this value. For isotropic turbulence the small-scale flatness increases. This departure from Gaussianity characterizes an increased intermittency in the small scales. The longitudinal flatness is smaller than the transversal flatness.

An explanation for the increase of intermittency as a function of scale can be given starting with the theory of stochastic distortion of turbulence, proposed by Nazarenko *et al.* [15] for the dynamo problem and Dubrulle *et al.* [16] for Navier-Stokes turbulence. According to their model, small-scale wave packets (in our case wavelets), initially isotropically distributed, get deformed by small-wave-number-induced strain. This results in cactus-leaf-shaped distributions with one small, one large, and one neutral axis. The energy at the tops of the cactus leaf, near the ends of the long axis, are more dissipated than the other ones. This process repeats itself in randomly oriented directions, so that after some deformations, a highly irregular, fingered energy distribution is obtained in Fourier space. The intermittent distribution of the small scales corresponds to the increased flatness at high wave numbers. If we consider now one particular component of the velocity field, which has the shape of an 8 in two dimensions (Fig. 4), the transversal direction, containing the larger part of the two lobes of the 8 shape, reaches higher wave numbers than the longitudinal direction, so that this fingering effect due to stochastic straining is stronger in the transversal direction: the transversal small-scale flatness is larger than the longitudinal flatness. Using the direct link between Fourier space and wavelet-space (Fig. 2), this mechanism could be applied to explain the present results, shown in Fig. 6.

The rotating turbulence shows a behavior very similar to the isotropic case: the longitudinal flatness is smaller than the transversal flatness. For the stratified case, the picture is different: the flatness in the z direction behaves approximately as for the isotropic case. However, the flatness in the x and y directions increases dramatically with scale. We need an additional mechanism to explain this. In stratified turbulence the energy tends to concentrate around the vertical wave vector: the dyadic cones around the horizontal plane $k_z=0$ in Fourier space are almost completely depleted from energy [6,20]. The rare fluctuations of energy in these directions correspond to an extreme intermittency: in stratified turbulence the small-scale intermittency is highly anisotropic. For the u component, it is also possible to partially explain the results by the nonlocal strain mechanism, described in the previous paragraph: the longitudinal directional flatness (in the x direction) is smaller than the transversal one (in the y direction), with x and y both perpendicular to the direction of stratification.

The observations can thus be explained by two competing mechanisms. First, the nonlocal strain that induces an anisotropy in the intermittency because the variance of the different components of a divergence-free vector field is anisotropically distributed in Fourier space. Second, the energy depletion of the horizontal plane in Fourier space due to the influence of stratification. Rotation is shown not to play a major role in the amplification or damping of small-scale intermittency in Fourier space.

V. CONCLUSION

To summarize, the present results reconfirm the picture [6,20] that for stratified turbulence, energy accumulates in a cone around the vertical axis in Fourier space and toward a horizontal plane for rotating flow. The introduction of a statistical diagnostic, the directional scale-dependent flatness, allows us to obtain a more precise picture of the spatial fluctuations of this spectral energy distribution. The simulations allowed us to focus on small-scale intermittency, which was shown to be highly anisotropic. The transversal flatness is larger than the longitudinal flatness, which can be explained by a nonlocal straining of the small scales by the large scales combined with the energy distribution in Fourier space resulting from the incompressibility constraint. In stratified turbulence, this effect is overshadowed by an energy depletion of the horizontal plane in Fourier space.

The present results may have implications for the development of models for anisotropic turbulence. A sound physical model—e.g., an anisotropic extension of the advected delta-vee system [21] or the models proposed in [22,23]—should address the anisotropy of the departure from Gaussianity of the small scales. Future studies could address the influence of Reynolds, Froude, and Rossby numbers on the anisotropy at small scales as well as in the inertial range.

ACKNOWLEDGMENTS

Stimulating interaction with Claude Cambon, Marie Farge, and Fabien Godeferd is acknowledged. This work was supported by the Agence Nationale de la Recherche under Contract No. M2TFP.

[1] G. I. Taylor, Proc. R. Soc. London **164**, 476 (1938).
[2] A. A. Townsend, Aust. J. Sci. Res., Ser. A **1**, 161 (1948).
[3] V. A. Sandborn, J. Fluid Mech. **6**, 221 (1959).
[4] G. K. Batchelor and A. A. Townsend, Proc. R. Soc. London **199**, 238 (1949).
[5] J. J. Riley, R. W. Metcalfe, and M. A. Weissman, in *Nonlinear Properties of Internal Waves*, edited by Bruce J. West, AIP Conf. Proc. No. 76 (AIP, New York, 1981), p. 79.
[6] F. S. Godeferd and C. Cambon, Phys. Fluids **6**, 2084 (1994).
[7] C. Cambon, Eur. J. Mech. B/Fluids **20**, 489 (2001).
[8] C. Brun and A. Pumir, Phys. Rev. E **63**, 056313 (2001).
[9] R. H. Kraichnan, Phys. Fluids **10**, 2080 (1967).
[10] I. Arad, V. S. L'vov, and I. Procaccia, Phys. Rev. E **59**, 6753 (1999).
[11] A. Babiano, C. Basdevant, and R. Sadourny, J. Atmos. Sci. **42**, 941 (1985).
[12] K. Schneider, M. Farge, and N. Kevlahan, *Woods Hole Mathematics: Perspectives in Mathematics and Physics*, edited by N. Tongring and R. C. Penner (World Scientific, Singapore, 2004), pp. 302–328.
[13] C. Meneveau, J. Fluid Mech. **232**, 469 (1991).
[14] M. Farge, Y. Guezennec, C. M. Ho, and C. Meneveau, *CTR Summer Program 1990* (NASA/Stanford University, Stanford, CA 1990), pp. 331–343.
[15] S. Nazarenko, R. J. West, and O. Zaboronski, Phys. Rev. E **68**, 026311 (2003).
[16] B. Dubrulle, J.-P. Laval, S. Nazarenko, and O. Zaboronski, J. Fluid Mech. **520**, 1 (2004).
[17] L. Liechtenstein, F. S. Godeferd, and C. Cambon, J. Turbul. **6**, 1 (2005).
[18] M. Farge, Annu. Rev. Fluid Mech. **24**, 395 (1992).
[19] S. Mallat, *A Wavelet Tour of Signal Processing* (Academic Press, San Diego, 1998).
[20] C. Cambon and L. Jacquin, J. Fluid Mech. **202**, 295 (1989).
[21] Y. Li and C. Meneveau, Phys. Rev. Lett. **95**, 164502 (2005).
[22] M. Chertkov, A. Pumir, and B. I. Shraiman, Phys. Fluids **11**, 2394 (1999).
[23] L. Chevillard and C. Meneveau, Phys. Rev. Lett. **97**, 174501 (2006).